INTERNATIONAL JOURNAL FOR NUMERICAL METHODS IN FLUIDS
Int. J. Numer. Meth. Fluids 2001; **37**: 249–277 (DOI: 10.1002/fld.169)

Absorbing boundary condition on elliptic boundary for finite element analysis of water wave diffraction by large elongated bodies

Subrata Kumar Bhattacharyya*, Santhosh Sathyapal and Chiruvai P. Vendhan

Ocean Engineering Centre, Indian Institute of Technology, Madras, India

SUMMARY

In a domain method of solution of exterior scalar wave equation, the radiation condition needs to be imposed on a truncation boundary of the modelling domain. The Bayliss, Gunzberger and Turkel (BGT) boundary dampers of first- and second-orders, which require a circular cylindrical truncation boundary in the diffraction-radiation problem of water waves, have been particularly successful in this task. However, for an elongated body, an elliptic cylindrical truncation boundary has the potential to reduce the modelling domain and hence the computational effort. Grote and Keller [On non-reflecting boundary conditions. *Journal of Computational Physics* 1995; **122**: 231–243] proposed extension of the first- and second-order BGT dampers for the elliptic radiation boundary and used these conditions to the acoustic scattering by an elliptic scatterer using the finite difference method. In this paper, these conditions are implemented for the problem of diffraction of water waves using the finite element method. Also, it is shown that the proposed extension works well only for head-on wave incidence. To remedy this, two new elliptic dampers are proposed, one for beam-on incidence and the other for general wave incidence. The performance of all the three dampers is studied using a numerical example of diffraction by an elliptic cylinder. Copyright © 2001 John Wiley & Sons, Ltd.

KEY WORDS: absorbing boundary condition; elliptic boundary damper; elongated bodies; finite element method; wave diffraction

1. INTRODUCTION

Linear diffraction of small amplitude free surface water waves by large bodies is a well-understood problem. This can be accurately solved by various numerical methods, e.g. the boundary integral, finite difference method (FDM) and finite element method (FEM). In a domain method such as the FEM, the infinite fluid domain involved in the problem has to be limited to a finite domain in which computations are carried out. This requires setting up of a

* Correspondence to: Ocean Engineering Centre, Indian Institute of Technology Madras, Chennai, Madras 600 036, India.

Received November 1999
Revised February 2000

truncation boundary around the body at some distance from it where the radiation condition is imposed by an approximate absorbing boundary condition (ABC). Many such approximations have been tried out, a review of which may be found in Givoli [1] and Emson [2]. Of these options, the approximations provided by boundary dampers (BD) based upon the Bayliss, Gunzburger and Turkel (BGT) [3] boundary conditions have been proved to be very efficient and accurate [4,5]. These dampers have been used not only in water wave diffraction and radiation problems, but also in several other fields of engineering where solution of the exterior scalar wave equation (Helmholtz equation) is necessary, e.g. scattering of acoustic and electromagnetic waves.

The three-dimensional problem domain Ω is defined by an inner domain Ω_I that encompasses the scatterer(s) and an outer domain Ω_O separated by the fictitious cylindrical truncation (or radiation) surface S_R as shown in Figure 1. The boundary curve Γ_R defines the shape of S_R in the xy plane demarcating the inner and outer areas (S_I and S_O) in the xy plane around the body (see Figure 2). Any ABC is good enough for numerical modelling if S_R is far away from the body surface S_B. In other words, if the computational fluid domain (Ω_I) is large enough, it will yield accurate results. However, the performance of an ABC is determined by the distance of S_R from S_B, of which r_B (i.e. radius of S_R) is a measure (see Figure 2(a)). For the same accuracy, the ABC that requires less r_B is better, since it implies smaller S_I. The appropriate value of r_B depends on the frequency of the incident wave and can therefore be related to the wavelength to measure the performance of an ABC. Scatterers have to be enclosed within a circular cylindrical domain for three-dimensional water wave diffraction, two-dimensional acoustic and electromagnetic problems and within a spherical domain for three-dimensional acoustic and electromagnetic problems. The reason for this is that the two-dimensional and three-dimensional BDs of the BGT type have been developed in the literature in circular and spherical co-ordinates.

If the body (i.e. the scatterer) is of elongated shape, enclosing it in a circular cylindrical truncation domain (i.e. Γ_R is a circle, Figure 2(a)) in the diffraction problem of water waves evidently results in a large computational domain, whose measure is S_I. On the other hand, if the Γ_R boundary is elliptic (Figure 2(b)), the size of S_I reduces significantly. To achieve this,

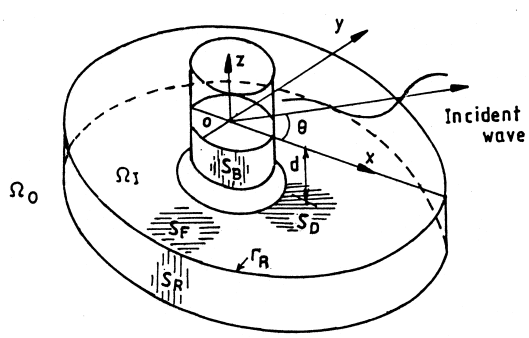

Figure 1. Wave diffraction problem.

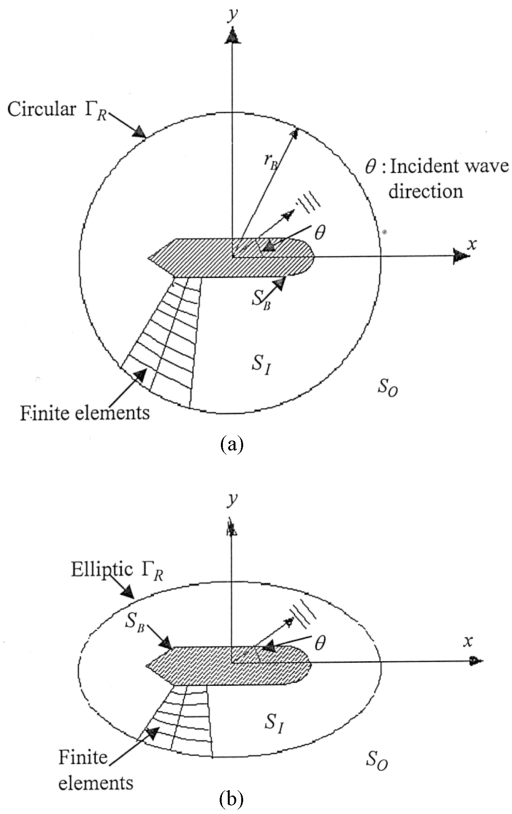

Figure 2. Definition sketch. (a) Circular cylindrical radiation boundary. (b) Elliptic cylindrical radiation boundary.

one has to develop ABCs on an elliptic Γ_R boundary. Grote and Keller [6] developed both first- and second-order elliptic boundary dampers based upon the BGT-type first- and second-order damper operator and used it in two-dimensional acoustic problems in conjunction with the FDM. Burnett and Holford [7] presented a new three-dimensional time-harmonic spheroidal family (prolate and oblate) of acoustic infinite elements for modelling acoustic fields in exterior domains. These elements are based on multipole expansion for acoustic field in spheroidal co-ordinates. They further developed a three-dimensional ellipsoidal infinite element, which is a logical generalization of the spheroidal infinite elements for solving acoustic problems involving elongated bodies [8]. The objectives of the present paper are threefold. Firstly, we implement the damper developed by Grote and Keller [6] for the diffraction problem of water waves in conjunction with the FEM. Secondly, we propose two new dampers based upon the same approach taken by them, which are more effective in such problems. Thirdly, we provide derivations of all the three dampers, discuss their finite element implementation and study their numerical performance on a comparative basis.

2. THE ELLIPTIC DAMPER FORMULATION

Consider the diffraction of small amplitude free surface waves by large obstacles. Assuming the fluid to be ideal and motion irrotational, linear harmonic water wave propagation is governed by the three-dimensional Laplace equation (see Figure 1) [14]

$$\frac{\partial^2\phi_t}{\partial x^2}+\frac{\partial^2\phi_t}{\partial y^2}+\frac{\partial^2\phi_t}{\partial z^2}=0 \quad \text{in } \Omega_I \tag{1a}$$

where $\phi_t(x, y, z)$ is the velocity potential which can be expressed as the sum of incident potential ϕ_I and scattered potential ϕ (i.e. $\phi_t=\phi_I+\phi$). The scattered potential should also satisfy the following boundary conditions:

$$\frac{\partial\phi}{\partial z}-\frac{\omega^2}{g}\phi=0 \quad \text{on the free surface } S_F \tag{1b}$$

where ω is the angular frequency of the wave and g is the acceleration due to gravity

$$\frac{\partial\phi}{\partial n}=-\frac{\partial\phi_I}{\partial n} \quad \text{on the body surface } S_B \tag{1c}$$

where n denotes normal to the body surface

$$\frac{\partial\phi}{\partial z}=0 \quad \text{on the sea bed } S_D \tag{1d}$$

It is well known that the scattered waves (as well as radiated waves in the case of floating bodies with no forward speed) in general consist of a propagating wave and an infinite number of evanescent modes [9], the latter wave forms having a strong decay in the vicinity of the body. Consider a surface S_R (see Figure 1) so located that the evanescent modes have insignificant amplitudes at this surface. Now, considering the fluid domain Ω_O bounded only by S_R, and assuming an impervious seabed (S_D, see Figure 1) and constant water depth (d, see Figure 1) in Ω_O, the scattered velocity potential may be expressed in the form [9]

$$\phi(x, y, z)=f_0(z)\phi_0(x, y)=\cosh k(z+d)\phi_0(x, y) \tag{2}$$

where k ($=2\pi/L$) is the wave number and L is the wavelength. Then, substituting Equation (2) into Equation (1a) and noting that $\nabla^2\phi_I=0$, we obtain the two-dimensional Helmholtz equation in terms of ϕ_0 as

$$\frac{\partial^2\phi_0}{\partial x^2}+\frac{\partial^2\phi_0}{\partial y^2}+k^2\phi_0=0 \quad \text{in } S_O \tag{3}$$

A boundary condition at infinity is required to solve such unbounded domain problems. This condition is the so-called Sommerfeld radiation condition, which is given in the form of a limit. It is difficult to incorporate such a limiting condition directly in any numerical procedure such as the FDM or FEM. Therefore, in these domain methods we define a finite computational domain Ω_I, which is bounded internally by the body surface S_B and externally by an artificial truncation boundary S_R (see Figure 1). This artificial boundary is a source of spurious reflections unless the infiniteness of the domain is properly accounted for. One of the most promising methods of imposing the boundary condition on the truncation boundary is by using a hierarchy of boundary dampers in the finite element formulation. The effectiveness of the plane and BGT-type cylindrical dampers of first- and second-order in diffraction problems of water waves has first been brought out by Bando *et al.* [4]. The use of these dampers will become inefficient for problems involving highly elongated bodies since the extent of the cylindrical computational domain increases unacceptably. Hence, one has to derive conditions applicable on boundaries that define economical computational domains such as elliptic boundaries.

Now consider the general case of an elliptic truncation boundary (Figure 2(b)). In this case, the exterior boundary Γ_R will be an ellipse defined by semi-major axis (a), semi-minor axis (b) and semi-inter focal distance (h) (see Figure 3). The radiation condition will be formulated in

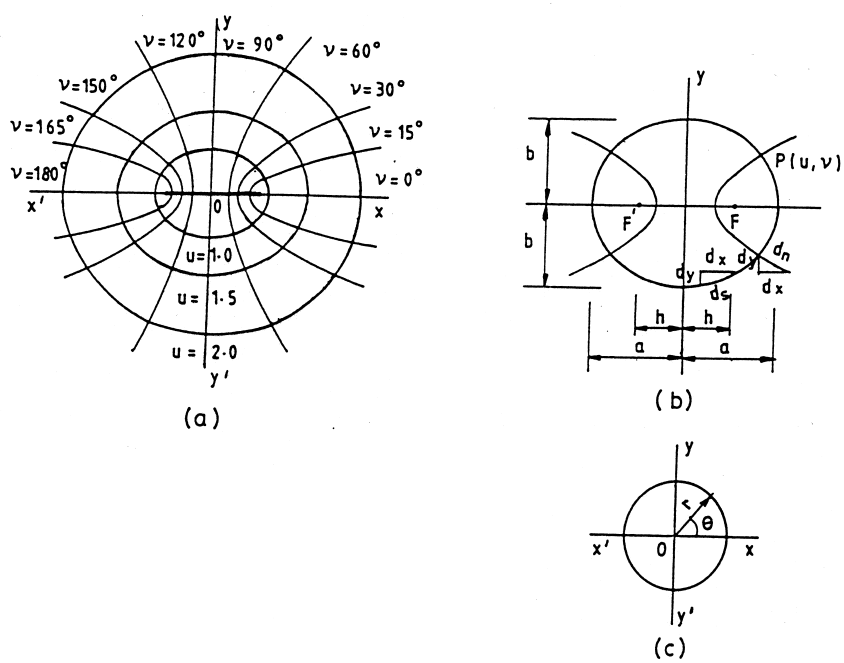

Figure 3. Elliptic co-ordinate system. (a) Orthogonally intersecting ellipse and hyperbola. (b) Normal and tangent to elliptic boundary. (c) Degenerate form of ellipse (circle) when $h = 0$.

an elliptic co-ordinate system. The relations between the cartesian (x, y) and elliptic (u, v) co-ordinates are [10]

$$x = h \cosh u \cos v, \qquad y = h \sinh u \sin v \quad (0 \le u < \infty,\ 0 \le v \le 2\pi) \tag{4}$$

The constant u curves are a set of confocal ellipses with semi-major axis $a = h \cosh u$, semi-minor axis $b = h \sinh u$ and foci at $(x, y) = (\pm h, 0)$. The eccentricity of the ellipse is then $e = 1/\cosh u$. The constant v curves are a set of confocal hyperbolas with the same foci. The well-known equations of these orthogonal conics are

$$\left(\frac{x}{h \cosh u}\right)^2 + \left(\frac{y}{h \sinh u}\right)^2 = 1 \quad \text{(ellipse)}, \qquad \left(\frac{x}{h \cos v}\right)^2 - \left(\frac{y}{h \sin v}\right)^2 = 1 \quad \text{(hyperbola)}$$

Next, we cast the Helmholtz equation (3) in terms of the elliptic co-ordinates (u, v). Towards this we define

$$z = x + \mathrm{i}y \quad (\mathrm{i} = \sqrt{-1}) \tag{5a}$$

$$w = u + \mathrm{i}v \quad (\mathrm{i} = \sqrt{-1}) \tag{5b}$$

It can be readily verified that

$$4 \frac{\partial^2 z z^*}{\partial z\, \partial z^*} = \left(\frac{\partial^2}{\partial x^2} + \frac{\partial^2}{\partial y^2}\right) z z^* \tag{6a}$$

$$4 \frac{\partial^2 w w^*}{\partial w\, \partial w^*} = \left(\frac{\partial^2}{\partial u^2} + \frac{\partial^2}{\partial v^2}\right) w w^* \tag{6b}$$

by noting that both left-hand side (LHS) and right-hand side (RHS) of the above two equations (where an * denotes a complex conjugate) equal 4. Substituting Equation (4) into Equation (5a) and using Equation (5b) and doing a similar operation on z^*, we get $z = h \cosh w$, $z^* = h \cosh w^*$, using

$$\frac{\partial}{\partial z} = \frac{\partial w}{\partial z} \frac{\partial}{\partial w} = \frac{1}{h \sinh w} \frac{\partial}{\partial w}; \qquad \frac{\partial}{\partial z^*} = \frac{\partial w^*}{\partial z} \frac{\partial}{\partial w^*} = \frac{1}{h \sinh w^*} \frac{\partial}{\partial w^*} \tag{7}$$

Substituting Equation (7) into the operator of Equation (6a) and noting the operator in Equation (6b), we get

$$\frac{\partial^2}{\partial x^2} + \frac{\partial^2}{\partial y^2} = 4 \frac{\partial^2}{\partial z\, \partial z^*} = \frac{4}{h^2 \sinh w \sinh w^*} \frac{\partial^2}{\partial v^2} = \frac{1}{h^2(\cosh^2 u - \cos^2 v)} \left(\frac{\partial^2}{\partial u^2} + \frac{\partial^2}{\partial v^2}\right) \tag{8}$$

Substituting Equation (8) into Equation (3), we get the Helmholtz equation in elliptic co-ordinates as

$$\frac{\partial^2\phi_0}{\partial u^2}+\frac{\partial^2\phi_0}{\partial v^2}+k^2h^2(\cosh^2 u-\cos^2 v)\phi_0=0 \tag{9}$$

Grote and Keller [6] derived an asymptotic representation of the solution for large u and they observed that the solution is identical to the asymptotic expansion in polar co-ordinates (r, θ) with r replaced by $h\cosh u$. The sequence of local operators, B_m for the BGT dampers in polar co-ordinates is [3,4]

$$B_m=\prod_{l=m}^{1}\left(\frac{\partial}{\partial r}-\mathrm{i}k+\frac{2l-3/2}{r}\right), \qquad B_m\phi_0=O(r^{-(2m+1/2)}) \tag{10}$$

When the eccentricity of an ellipse with constant a approaches zero (i.e. $e\to 0$), the ellipse approaches a circle of radius $r=a$. In this limit, $u\to\infty$ (since $\cosh u=1/e$), $h\to 0$ (since $h=ae$), i.e. the foci coalesce to the origin of the circle ($x=y=0$) and $h\sinh u\to h\cosh u\to r$. If $r=h\cosh u$, we have

$$\frac{\partial r}{\partial u}=h\sinh u, \qquad \frac{\partial}{\partial u}=h\sinh u\frac{\partial}{\partial r}$$

which, on substitution into Equation (10), gives

$$B_m=\prod_{l=m}^{1}\left(\frac{1}{h\sinh u}\frac{\partial}{\partial u}-\mathrm{i}k+\frac{2l-3/2}{h\cosh u}\right), \qquad B_m\phi_0=O((h\cosh u)^{-(2m+1/2)}) \tag{11}$$

This is the form of the BGT local operators in elliptic co-ordinates as presented by Grote and Keller [6], which henceforth are called the Grote and Keller (GK) operators and the dampers based upon it, the GK dampers.

Thus, the boundary condition to be implemented is

$$B_m\phi_0=0 \quad \text{on } \Gamma_R \text{ (in Figure 2)} \tag{12}$$

where the order of error is as given by the second of Equation (10) with r replaced by $h\cosh u$ for a given m. Though the accuracy can be improved by increasing m, the dampers up to $m=2$ are only viable because of the complexity in the formulation and implementation associated with dampers with $m>2$. In the finite element formulation it is more appropriate to express the above condition in the form of a Neumann condition of the following form:

$$B_m\phi_0=\frac{\partial\phi_0}{\partial n}-S_m\phi_0=0 \quad \text{on } \Gamma_R \text{ (in Figure 2)} \tag{13a}$$

where S_m is the damper operator. In view of Equation (2), Equation (13a) may also be written in terms of the three-dimensional scattered velocity potential as

$$B_m\phi = \frac{\partial \phi}{\partial n} - S_m\phi = 0 \quad \text{on the surface } S_R \text{ (in Figure 1)} \tag{13b}$$

Bando *et al*. [4] and Clark *et al*. [11] have presented finite element analysis of wave diffraction by cylinders using the damper equation (13a). Krishnankutty and Vendhan [5] employed the version in Equation (13b) in terms of the three-dimensional potential and validated the numerical performance of such damper equations employed on S_{R} in the form of a circular cylindrical surface (Figure 1). The present paper is concerned with similar studies with S_{R} in the form of an elliptic cylinder.

2.1. First-order GK damper

To obtain the first-order radiation condition on an elliptic boundary, we set $m = 1$ in Equation (11) and use Equation (12) for B_1 operator to yield

$$\frac{\partial \phi_0}{\partial u} + \left(\frac{1}{2}\tanh u - \mathrm{i}kh \sinh u\right)\phi_0 = 0 \tag{14}$$

Referring to Figure 3(b), the arc length dn defined along a constant v curve (i.e. normal to the ellipse) is

$$\mathrm{d}n = \left[\left(\frac{\partial x}{\partial u}\right)^2 + \left(\frac{\partial y}{\partial u}\right)^2\right]^{1/2} \mathrm{d}u = l_1 \,\mathrm{d}u \tag{15}$$

Thus

$$\frac{\partial}{\partial n} = \frac{1}{l_1}\frac{\partial}{\partial u} \tag{16}$$

From Equation (4), $\partial x/\partial u = h \sinh u \cos v$ and $\partial y/\partial u = h \cosh u \sin v$, using Equation (15) leads to

$$l_1 = h(\cosh^2 u - \cos^2 v)^{1/2} \tag{17}$$

In view of Equation (16), Equation (14) can be written as

$$\frac{\partial \phi_0}{\partial n} + \alpha\phi_0 = 0 \tag{18a}$$

where

$$\alpha = \frac{1}{l_1}\left(\frac{1}{2}\tanh u - \mathrm{i}kh \sinh u\right) \tag{18b}$$

Equation (18) represents the first-order radiation condition for outgoing waves on an elliptic truncation boundary. Rewriting Equation (18) in the form of a Neumann condition in Equation (13b), we have

$$\frac{\partial \phi}{\partial n} - S_1 \phi = O\left(\frac{1}{(h \sinh u)^{5/2}}\right), \quad S_1 = -\alpha \tag{18c}$$

where S_1 is the first-order damper operator. It may be noted that when the elliptic boundary reduces to a circular one ($h = 0$), $h \sinh u = h \cosh u = r$; $l_1 = r$ as $h \cos v = 0$ and $\tanh u = 1$ so that the factor α becomes

$$\alpha = \frac{1}{2r} - \mathrm{i}k \tag{19}$$

which is the standard form of the BGT-type first-order cylindrical damper [4,12].

2.2. Second-order GK damper

To obtain the second-order radiation condition on an elliptic boundary, we set $m = 2$ in Equation (11) and use Equation (12) for the B_2 operator to yield

$$B_2 \phi_0 = \left(\frac{1}{h \sinh u}\frac{\partial}{\partial u} - \mathrm{i}k + \frac{5}{2h \cosh u}\right)\left(\frac{1}{h \sinh u}\frac{\partial}{\partial u} - \mathrm{i}k + \frac{1}{2h \cosh u}\right)\phi_0 = 0$$

which on simplification gives

$$\frac{\partial^2 \phi_0}{\partial u^2} + (3 \tanh u - 2\mathrm{i}kh \sinh u - \coth u)\frac{\partial \phi_0}{\partial u} + \left(\frac{3}{4}\tanh^2 u - (kh \sinh u)^2 - 3\mathrm{i}kh \sinh u \tanh u\right)\phi_0 = 0 \tag{20}$$

The above equation contains second-order derivative with respect to u, which may lead to difficulties in FEM. In order to eliminate such terms we consider the elliptic arc length (i.e. distance along the constant u curve) ds, which is given by (see Figure 2(b))

$$\mathrm{d}s = \left[\left(\frac{\partial x}{\partial u}\right)^2 + \left(\frac{\partial y}{\partial u}\right)^2\right]\mathrm{d}v = l_1 \, \mathrm{d}v \tag{21}$$

where l_1 is given by Equation (17). Considering Equations (15) and (21), it is clear that dn and ds are normal and tangential (infinitesimal) arc lengths on the constant u curve. The above relation gives

$$\frac{\partial}{\partial v} = l_1 \frac{\partial}{\partial s} \tag{22}$$

and hence

$$\frac{\partial^2}{\partial v^2} = l_1 \frac{\partial}{\partial s}\left(l_1 \frac{\partial}{\partial s}\right) = l_1^2 \frac{\partial^2}{\partial s^2} + l_1 \frac{\partial l_1}{\partial s}\frac{\partial}{\partial s}$$

$$= l_1^2 \frac{\partial^2}{\partial s^2} + l_1\left(\frac{1}{l_1}\frac{\partial l_1}{\partial v}\right)\frac{\partial}{\partial s} \quad \text{using Equation (22)}$$

$$= l_1^2 \frac{\partial^2}{\partial s^2} + \frac{h^2 \sin 2v}{2l_1}\frac{\partial}{\partial s} \quad \text{using Equation (17)} \tag{23}$$

Now, substituting $\partial^2/\partial u^2$ from the Helmholtz equation (9) and $\partial/\partial u$ from Equation (16) into Equation (20) and then replacing $\partial^2/\partial v^2$ in the resulting equation by Equation (23), we get

$$\frac{\partial \phi}{\partial n} + \alpha\phi - \beta \frac{\partial^2 \phi}{\partial s^2} - \beta \frac{h^2 \sin 2v}{2l_1^3}\frac{\partial \phi}{\partial s} = 0 \tag{24}$$

Comparing the above with Equation (13b) for $m = 2$, we get

$$S_2 = -\alpha + \beta \frac{\partial^2}{\partial s^2} + \beta \frac{h^2 \sin 2v}{2l_1^3}\frac{\partial}{\partial s} \tag{25}$$

where

$$\alpha = \frac{\frac{3}{4}\tanh^2 u - (kh \sinh u)^2 - 3ikh \sinh u \tanh u - k^2 l_1^2}{l_1(3 \tanh u - 2ikh \sinh u - \coth u)} \tag{26a}$$

and

$$\beta = \frac{l_1}{3 \tanh u - 2ikh \sinh u - \coth u} \tag{26b}$$

As the ellipse tends to a circle, substituting $h \sinh u = h \cosh u = l_1 = r$ and $\tanh u = \coth u = 1$ into Equation (26) we get

$$\alpha = \frac{\frac{3}{4r^2} - \frac{3ik}{r} - 2k^2}{\frac{2}{r} - 2ik} \tag{27a}$$

$$\beta = \frac{1}{\frac{2}{r} - 2ik} \tag{27b}$$

which match with the second-order BGT-type cylindrical dampers [4,12].

3. FIRST NEW DAMPER

The GK damper operators in Equation (11) were obtained by replacing r by $h\cosh u$ in the BGT damper operators in Equation (10). This is true in the limit when the ellipse approaches a circle and hence $r \to h\cosh u$. Also, since $r \to h\sinh u$ in the limit, a set of damper operators can also be derived by replacing r by $h\sinh u$ in Equation (10). For an ellipse which is distinct from a circle (i.e. $h \neq 0$), $r = h\cosh u$ holds at points $(x, y) = (\pm a, 0)$ and $r = h\sinh u$ holds at points $(x, y) = (0, \pm b)$. Hence, it is intuitively clear that the GK damper will perform well for waves incident on the body with a 0° or 180° angle of incidence ($\theta = 0°$ or 180°), i.e. for waves aligned with the x-axis. By the same token, it can be intuitively expected that the damper being proposed, which we will designate as the 'Damper 1' (D1) in what follows, will perform well, i.e. better than the GK dampers, for $\theta = 90°$ or 270°, when the incident waves are aligned with the y-axis. It will be shown later by numerical results that this indeed is the case. It may be well to point out at this stage that in the paper by Grote and Keller [6], the damper was numerically tested for an acoustic scattering problem only for $\theta = 0°$, an incidence angle where its performance should be the best.

Replacing r by $h\sinh u$ in Equation (10), it is easy to see that

$$B_m = \prod_{l=m}^{1} \left(\frac{1}{h\cosh u}\frac{\partial}{\partial u} - \mathrm{i}k + \frac{2l - 3/2}{h\sinh u} \right) \tag{28}$$

We call the operators in Equation (28) D1 operators. Setting $B_m\phi_0 = 0$ and following similar steps as in Sections 2.1 and 2.2, a set of new absorbing conditions for an elliptic radiation boundary can be derived. The first-order condition derived by setting $B_1\phi_0 = 0$ is analogous to Equation (18), with the coefficient α given by the following expression:

$$\alpha = \frac{1}{l_1}\left(\frac{1}{2}\coth u - \mathrm{i}kh\cosh u \right) \tag{29}$$

and the order of error as $(h\cosh u)^{-5/2}$, which is analogous to Equation (18c).

The second-order condition derived by setting $B_2\phi_0 = 0$ results in an equation analogous to Equation (24) with the following expressions for the coefficients α and β:

$$\alpha = \frac{\frac{3}{4}\coth^2 u - (kh\cosh u)^2 - 3\mathrm{i}kh\coth u\cosh u - k^2 l_1^2}{l_1(3\coth u - 2\mathrm{i}kh\cosh u - \tanh u)} \tag{30a}$$

and

$$\beta = \frac{l_1}{3\coth u - 2\mathrm{i}kh\cosh u - \tanh u} \tag{30b}$$

Comparing Equation (18b) with Equation (29) and Equation (26) with Equation (30), it is clear that the coefficients α and β of the D1 damper can readily be obtained from those of the GK damper by simply interchanging $\sinh u$ with $\cosh u$ and $\tanh u$ with $\coth u$ in the expressions. In the limiting case of the ellipse (i.e. circle), the coefficients in Equations (29) and (30) readily reduce to those of the cylindrical dampers given in Equations (19) and (27).

4. SECOND NEW DAMPER

The GK damper is better suited for wave incidence in the x-direction and the D1 damper introduced in Section 3 is better suited for wave incidence in the y-direction. A general elliptic damper can therefore be derived by replacing r, the distance of a point on the elliptical S_R, by elliptic co-ordinates u and v. This relation is

$$r = \sqrt{x^2 + y^2} = \frac{h}{\sqrt{2}} (\cosh 2u + \cos 2v)^{1/2} \tag{31}$$

Again, intuitively speaking, such a replacement should work better than the GK and D1 dampers for all wave incidences not aligned with either the x- or y-axis but work as well as the GK damper for incidence angles $\theta = 0°$ and 180° and as well as the D1 damper for $\theta = 90°$ and 270°. It will be shown later numerically that this indeed is the case. Substituting Equation (31) for r into Equation (10), we get

$$B_m = \prod_{l=m}^{1} \left(\frac{\sqrt{2}}{h} \frac{(\cosh 2u + \cos 2v)}{\sinh 2u} \frac{\partial}{\partial u} - \mathrm{i}k + \frac{\sqrt{2}}{h} \frac{2l - 3/2}{(\cosh 2u + \cos 2v)^{1/2}} \right) \tag{32}$$

We call the operators in Equation (32) the 'Damper 2' (D2) operators. To obtain the new first-order boundary condition, set $m = 1$ and rewrite $B_1 \phi_0 = 0$. It can be seen that this results in an equation analogous to Equation (18a) with the coefficient α, for the D2 damper introduced herein, given by

$$\alpha = \frac{h^2 \sinh 2u}{2 l_1 r} \left(\frac{1}{2r} - \mathrm{i}k \right) \tag{33}$$

where l_1 and r are given by Equations (17) and (31), respectively.

To derive the second-order boundary condition, we set $m = 2$ and rewrite $B_2 \phi_0 = 0$. This requires some lengthy algebra and the resulting equation is analogous to Equation (24) with the coefficients α and β given by

$$\alpha = \frac{\dfrac{h^4 \sinh^2 2u}{4r^2} \left(\dfrac{3}{4r^2} - k^2 - \dfrac{3\mathrm{i}k}{r} \right) - k^2 l_1^2}{\dfrac{h^2 l_1 \sinh 2u}{r} \left(\dfrac{2}{r} - \mathrm{i}k \right) - 2 l_1 \coth 2u} \tag{34a}$$

$$\beta = \frac{1}{\dfrac{h^2 \sinh 2u}{r l_1}\left(\dfrac{2}{r} - \mathrm{i}k\right) - \dfrac{2}{l_1}\coth 2u} \tag{34b}$$

where again l_1 and r are given by Equations (17) and (31), respectively. It can be verified that by putting $r = h\cosh u$ or $h\sinh u$, α and β in Equations (33) and (34) reduce to the corresponding GK damper (Equations (18b) and (26)) and D1 damper (Equations (29) and (30)) expressions, respectively. In addition, in the limiting case when Γ_R is a circle, they reduce to the expressions for BGT-type cylindrical dampers given by Equations (19) and (27). Thus, the D2 damper formulation is more general covering all the boundary conditions derived earlier.

5. FINITE ELEMENT IMPLEMENTATION

The Laplace equation in terms of the scattered potential ϕ, the free surface boundary condition on S_F (Equation (1b)), the Neumann condition on the body surface S_B (Equation (1c)) and the radiation boundary condition in the form of ABC (i.e. Equation (13b)) discussed in Sections 2–4 can be put in an equivalent variational form. The associated functional $I(\phi)$ can be written as

$$I(\phi) = \frac{1}{2}\int_{\Omega_I} \nabla\phi\cdot\nabla\phi \, \mathrm{d}\Omega - \frac{\omega^2}{2g}\int_{S_F} \phi^2 \, \mathrm{d}S + I_R(\phi) + \int_{S_B} \frac{\partial\phi_I}{\partial n}\,\phi \, \mathrm{d}S \tag{35a}$$

where ω is the angular frequency of the wave, g is the acceleration due to gravity, ϕ_I is the linear velocity potential of the incident wave, n denotes the normal to the body surface (S_B), S_F is the free surface and $I_R(\phi)$ is a functional corresponding to the damper operator S_m defined in Equation (13b). Taking the first variation of Equation (35a) and setting it to zero, we get

$$\delta I(\phi) = \int_{\Omega_I} [\nabla\phi\cdot\delta(\nabla\phi)]\,\mathrm{d}\Omega - \frac{\omega^2}{g}\int_{S_F} \phi\delta\phi \, \mathrm{d}S + \delta I_R(\phi) + \int_{S_B} \frac{\partial\phi_I}{\partial n}\,\delta\phi \, \mathrm{d}S = 0 \tag{35b}$$

As the radiation conditions (first-order, Equation (18a) and second-order, Equation (24)) imposed on elliptic truncation boundary S_R are of primary concern in this paper, their finite element implementation is presented here in detail. Consider the following expression for $I_R(\phi)$ corresponding to the radiation condition in the variational statement, Equation (35a)

$$I_R(\phi) = \int_{S_R}\left[\frac{\alpha}{2}\phi^2 + \frac{\beta}{2}\left(\frac{\partial\phi}{\partial s}\right)^2\right]\mathrm{d}S \tag{36a}$$

where α and β have already been defined for various damper approximations (i.e. GK, D1 and D2 dampers) and $\beta = 0$ for all first-order dampers. Writing down the first variation of $I_R(\phi)$ using the identity

$$\delta I(\phi) = \frac{\partial I}{\partial \phi}\,\delta\phi + \frac{\partial I}{\partial(\partial\phi/\partial s)}\,\delta\left(\frac{\partial \phi}{\partial s}\right)$$

we get

$$\delta I_{\mathrm{R}}(\phi) = \int_{S_{\mathrm{R}}} \alpha\phi\delta\phi \; \mathrm{d}S + \int_{S_{\mathrm{R}}} \beta\,\frac{\partial\phi}{\partial s}\,\delta\left(\frac{\partial\phi}{\partial s}\right)\mathrm{d}S \tag{36b}$$

Performing by-part integration of the second integral in the above equation and noting that the elemental area $\mathrm{d}S = \mathrm{d}s\;\mathrm{d}z$, we get

$$\begin{aligned}\delta I_{\mathrm{R}}(\phi) &= \int_{S_{\mathrm{R}}} \alpha\phi\delta\phi \; \mathrm{d}S + \int_{-d}^{0}\int_{s_1}^{s_2} \beta\,\frac{\partial\phi}{\partial s}\,\frac{\partial(\delta\phi)}{\partial s}\,\mathrm{d}s\;\mathrm{d}z \\ &= \int_{S_{\mathrm{R}}} \alpha\phi\delta\phi \; \mathrm{d}S + \int_{-d}^{0} \beta\,\frac{\partial\phi}{\partial s}\,\delta\phi\Big|_{s_1}^{s_2}\mathrm{d}z - \int_{S_{\mathrm{R}}}\left(\beta\,\frac{\partial^2\phi}{\partial s^2} + \frac{\partial\beta}{\partial s}\,\frac{\partial\phi}{\partial s}\right)\delta\phi \; \mathrm{d}S\end{aligned}$$

where the second integral is evaluated at the limits of the variable s (i.e. at s_1 and s_2) and this term reduces to zero when S_{R} is a closed surface. If the problem possesses symmetry about one or two of the axes (x- and y-axes), the finite element domain will be such that the projection of S_{R} on the z-axis is a quadrant or one half of an elliptic curve. In such cases also the second term vanishes because of the condition $\partial\phi/\partial s = 0$ or $\delta\phi = 0$ on the symmetry axis, depending on whether ϕ is symmetric or antisymmetric. Hence, $\delta I_{\mathrm{R}}(\phi)$ can be written as

$$\delta I_{\mathrm{R}}(\phi) = \int_{S_{\mathrm{R}}}\left[\alpha\phi - \beta\,\frac{\partial^2\phi}{\partial s^2} - \frac{\partial\beta}{\partial s}\,\frac{\partial\phi}{\partial s}\right]\delta\phi \; \mathrm{d}S \tag{36c}$$

From Equations (26b), (30b) and (34b), it is evident that β can be written as

$$\beta = \frac{l_1}{f(u)} \tag{37}$$

where $f(u)$ is a function of the elliptic co-ordinate u. From Equation (22) one obtains

$$\begin{aligned}\frac{\partial\beta}{\partial s} &= \frac{1}{l_1}\,\frac{\partial\beta}{\partial v} = \frac{1}{l_1 f(u)}\,\frac{\partial l_1}{\partial v} = \frac{h^2\sin 2v}{2l_1^2 f(u)} \quad \text{from Equation (17)} \\ &= \frac{\beta h^2 \sin 2v}{2l_1^3} \quad \text{from Equation (37)}\end{aligned} \tag{38}$$

Substituting Equation (38) for $\partial\beta/\partial s$ into Equation (36c) and using the resulting expression for $\delta I_{\mathrm{R}}(\phi)$ in Equation (35b) generates the radiation boundary condition on S_{R} in the form given by Equation (24). Hence, the functional $I_{\mathrm{R}}(\phi)$ defined in Equation (36a) provides for the absorbing boundary condition on S_{R}, which can easily be incorporated into the finite element program by means of boundary dampers.

The well-known isoparametric finite element formulation [13] is used here to obtain an approximate solution to the variational equation. In this formulation an element in the local co-ordinate system is mapped to the curvilinear element in the global Cartesian co-ordinate system by means of a set of element shape functions, N_i^e. Thus, for an element, the finite element approximation is given by $\phi = \boldsymbol{N}^{eT}\boldsymbol{\phi}^e$, where $\boldsymbol{N}^e$ is the array of element shape functions and $\boldsymbol{\phi}^e$ is the array of unknown potential values at element nodes and the superscript T denotes matrix transpose. Two types of C^0 elements, hexahedron (brick) and pentahedron (wedge) (see Figure 4(a) and (b)), are used in this work. For the hexahedral element with eight or 20 nodes, the shape functions are given by [13]

$$N_i^e = \frac{1}{8}(1+\xi\xi_i)(1+\eta\eta_i)(1+\zeta\zeta_i)(\xi\xi_i+\eta\eta_i+\zeta\zeta_i-2) \quad (i=1, 2, ..., 8)$$

$$N_i^e = \frac{1}{4}(1-\xi^2)(1+\eta\eta_i)(1+\zeta\zeta_i) \quad (i=9, 11, 13, 15)$$

$$N_i^e = \frac{1}{4}(1-\eta^2)(1+\xi\xi_i)(1+\zeta\zeta_i) \quad (i=10, 12, 14, 16)$$

$$N_i^e = \frac{1}{4}(1-\zeta^2)(1+\xi\xi_i)(1+\eta\eta_i) \quad (i=17, 18, 19, 20) \tag{39a}$$

where (ξ, η, ζ) denotes local co-ordinates for an element.

For the pentahedral elements with six or 15 nodes, the shape functions are given by

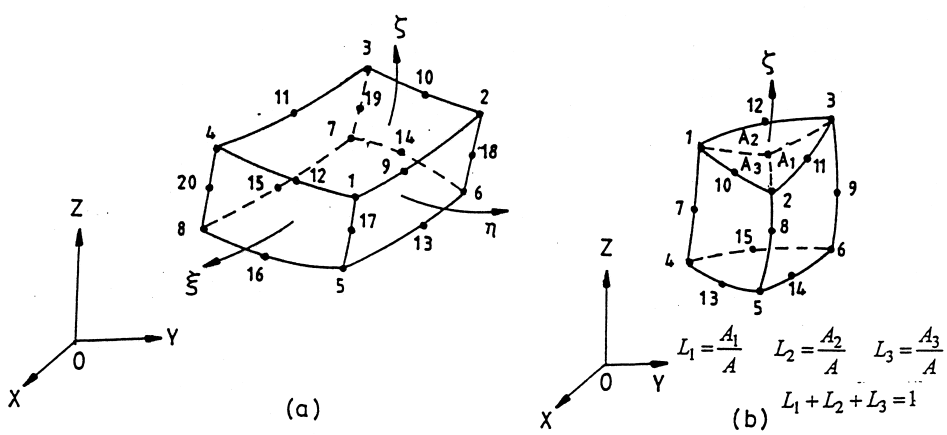

Figure 4. Finite elements used. (a) Eight or 20 noded hexahedron (brick). (b) Six or 15 noded pentahedron (wedge).

$$N_i^e = \frac{1}{2} L_1(2L_1 - 1)(1 + \zeta) - (1/2)L_1(1 - \zeta^2) \quad (i = 1, 2, \ldots, 6)$$

$$N_i^e = 2L_1L_2(1 + \zeta) \quad (i = 10, 11, \ldots, 15)$$

$$N_i^e = L_1(1 - \zeta^2) \quad (i = 7, 8, 9) \tag{39b}$$

where L_i, $i = 1, 2, 3$ are the area co-ordinates (with $L_1 + L_2 + L_3 = 1$) defining the triangular faces of the element and ζ is the natural co-ordinate along its length (see Figure 4(b)).

Now one can use the expression in Equation (36b) for $\delta I_R(\phi)$ and rewrite Equation (35b) as follows, after substituting the finite element approximation:

$$\sum_{el} \delta\boldsymbol{\phi}^{eT}\left(\int_{\Omega_I^e} \nabla \boldsymbol{N}^{eT} \nabla \boldsymbol{N}^e \, d\Omega\right)\boldsymbol{\phi}^e - \frac{\omega^2}{g} \sum_{el} \delta\boldsymbol{\phi}^{eT}\left(\int_{S_F^e} \boldsymbol{N}^{eT}\boldsymbol{N}^e \, dS\right)\boldsymbol{\phi}^e$$
$$+ \sum_{el} \delta\boldsymbol{\phi}^{eT}\left(\int_{S_R^e} \alpha \boldsymbol{N}^{eT}\boldsymbol{N}^e \, dS + \int_{S_R^e} \beta\left(\frac{\partial \boldsymbol{N}^e}{\partial s}\right)^T\left(\frac{\partial \boldsymbol{N}^e}{\partial s}\right) dS\right)\boldsymbol{\phi}^e + \sum_{el} \delta\boldsymbol{\phi}^{eT}\left(\int_{S_B^e} \boldsymbol{N}^{eT} \frac{\partial \boldsymbol{\phi}_I}{\partial n} \, dS\right) = 0 \tag{40}$$

In the above, bold characters denote vectors. The domains of integration correspond to the various finite elements and the summation denotes element assembly procedure carried out over all the elements. The global finite element equations can be deduced from this equation in the form [5]

$$(\boldsymbol{K}_\Omega + \boldsymbol{K}_F + \boldsymbol{K}_R)\boldsymbol{\phi} = \boldsymbol{f} \tag{41}$$

where the various global matrices are given by

$$\boldsymbol{K}_\Omega = \sum_{el} \int_{\Omega_I^e} \nabla \boldsymbol{N}^{eT} \nabla \boldsymbol{N}^e \, d\Omega, \qquad \boldsymbol{K}_F = -\frac{\omega^2}{g} \sum_{el} \int_{S_F^e} \boldsymbol{N}^{eT}\boldsymbol{N}^e \, dS$$

$$\boldsymbol{K}_R = \sum_{el}\left(\int_{S_R^e} \alpha \boldsymbol{N}^{eT}\boldsymbol{N}^e \, dS + \int_{S_R^e} \beta\left(\frac{\partial \boldsymbol{N}^e}{\partial s}\right)^T\left(\frac{\partial \boldsymbol{N}^e}{\partial s}\right) dS\right), \qquad \boldsymbol{f} = -\sum_{el} \int_{S_B^e} \boldsymbol{N}^{eT} \frac{\partial \phi_I}{\partial n} \, dS \tag{42}$$

where in the expression for $\boldsymbol{K}_R$ matrix, the derivative $(\partial \boldsymbol{N}^e/\partial s)$ is computed by chain rule of differentiation as

$$\frac{\partial \boldsymbol{N}^e}{\partial s} = \frac{\partial \boldsymbol{N}^e}{\partial x}\frac{\partial x}{\partial s} + \frac{\partial \boldsymbol{N}^e}{\partial y}\frac{\partial y}{\partial s} + \frac{\partial \boldsymbol{N}^e}{\partial z}\frac{\partial z}{\partial s} \tag{43}$$

with $(\partial x/\partial s, \partial y/\partial s, \partial z/\partial s)$ evaluated from the parametric formulation of the finite element. The matrix $\boldsymbol{K}_\Omega$ gets contribution from the inner domain Ω_I, whereas the matrices $\boldsymbol{K}_F$ and $\boldsymbol{K}_R$ get contributions only from the elements directly connected to the free surface and the truncation

boundary, respectively. The load vector $\boldsymbol{f}$ originates from elements directly connected to the body boundary. These matrices are formed by numerically evaluating the integrals using Gauss quadrature. The assembled global finite element equations (Equation (41)) represent a set of complex algebraic equations that can be solved for nodal potentials using the Gauss elimination algorithm suitable for large banded matrix equations.

6. SURFACE ELEVATION AND HYDRODYNAMIC FORCES

Hydrodynamic forces and moments due to wave diffraction are evaluated by integrating the hydrodynamic pressure over the body surface as given below

$$\boldsymbol{F} = -\int_{S_B} p\boldsymbol{n}\,\mathrm{d}S = \mathrm{i}\omega\rho \int_{S_B} (\phi_I + \phi)\boldsymbol{n}\,\mathrm{d}S \tag{44a}$$

and

$$\boldsymbol{M} = -\int_{S_B} p(\boldsymbol{r}\times\boldsymbol{n})\,\mathrm{d}S = \mathrm{i}\omega\rho \int_{S_B} (\phi_I + \phi)(\boldsymbol{r}\times\boldsymbol{n})\,\mathrm{d}S \tag{44b}$$

where p is the hydrodynamic pressure given by the linearized Bernoulli equation, ϕ_I the incident wave potential, $\boldsymbol{n}$ the outward normal vector to body surface (S_B), $\boldsymbol{r}$ denotes the position vector of a point on S_B and ρ the mass density of the fluid. The water surface elevation can be obtained in complex form as

$$\eta = \frac{\mathrm{i}\omega}{g}(\phi_I + \phi) = \eta_R + \mathrm{i}\eta_I \tag{45}$$

where the actual water surface elevation is given by $|\eta|$, which around the body surface is known as the wave run-up. The wave diffraction force and moments can be evaluated once the velocity potentials are known.

7. RESULTS AND DISCUSSION

The main thrust of the present numerical study has been to identify suitable aspect ratios of the Γ_R boundary, i.e. a_R/b_R, where a_R and b_R are a and b of the elliptic Γ_R, respectively (subscript R denotes the 'radiation boundary') and present a comparative performance study of the second-order versions of all three dampers applied to water wave diffraction problems. Minimal attention is given to the first-order dampers since they generally require larger Γ_R distance for comparable accuracy. The diffraction problem of prismatic vertical cylinders with elliptic cross section (see Figure 5) which extend from the sea bed to above the still water surface is employed in the numerical study because the diffracted waves in such a case consist only of propagating modes, which are implied in the radiation boundary condition and hence

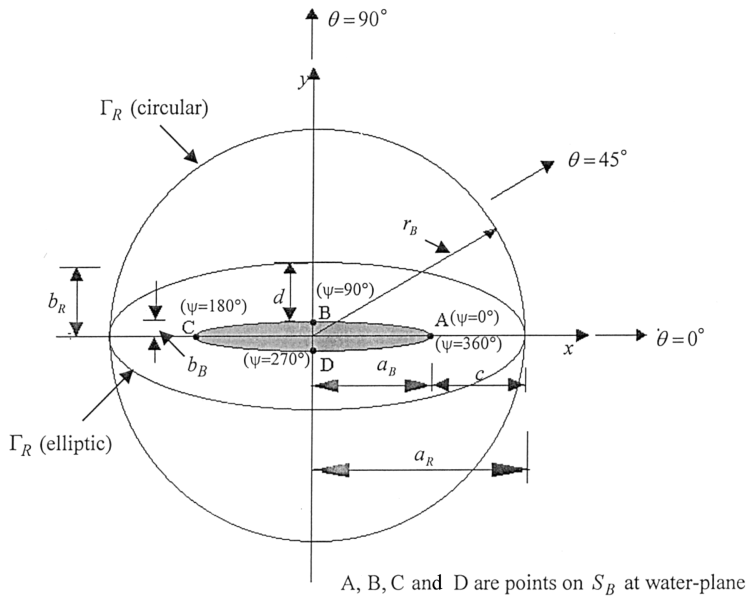

Figure 5. Elliptic cylinder of aspect ratio 8 showing three wave incidence angles and the dimensions of the body and radiation boundaries.

the boundary damper approximation. Since, in the literature an elliptic cylinder with aspect ratio 2 ($a_B/b_B = 2$) has been considered [4,11], this case is studied here for the purpose of validation using the dimensions given by Clark *et al.* [11]. However, an aspect ratio of 2 is too small for an elongated body and therefore an elliptic cylinder with aspect ratio 8 ($a_B/b_B = 8$) has been considered for detailed numerical study. This aspect ratio is sufficiently high for any elongated body likely to be encountered in practical applications. The details of the cases studied are (see Figure 5):

- cylinder dimensions: $a_B = 1$ m, $b_B = 0.125$ m, height $= 2$ m
- wave parameters: $(ka_B, L) = (3, 2.094$ m) and $(2\pi, 1$ m);
- wave height (H) = water depth $= 2$ m, water density $(\rho) = 1000$ kg m^{-3};
- wave incidence angles: $\theta = 0°$, 45° and 90°.

To set the geometrical perspective, we define $c = a_R - a_B$ and $d = b_R - b_B$, which are essentially the distances between the body and the radiation boundary (Γ_R) along the major and minor axes, respectively (see Figure 5). In most cases, $c/L = 0.5$ has been used in the calculations. The finite element mesh employed consists of at least five quadratic elements per wavelength in the radial direction (the minimum recommended being four in Bando *et al.* [4]) and 48 in the circumferential direction, though a somewhat smaller number could do as well.

Figure 6(a) presents the modelling domain for the elliptic cylinder of aspect ratio 2 with both circular and elliptic truncation boundaries for the three wave parameters $ka_B = 1, 2$ and 3. Figure 6(b) presents similar pictures for the elliptic cylinder of aspect ratio 8 for the two wave parameters $ka_B = 3$ and 2π.

The results presented for discussion are (i) wave diffraction force components F_x and F_y and the corresponding base moments M_y and M_x and (ii) wave run-up or surface elevation (η) around the cylinder ($\psi = 0°–360°$, see Figure 5). It may be noted that F_x and F_y are the components of $\boldsymbol{F}$ as defined in Equation (44a) and M_x and M_y are the components of $\boldsymbol{M}$ as defined in Equation (44b) with the co-ordinate origin at free surface (see Figure 1). While the

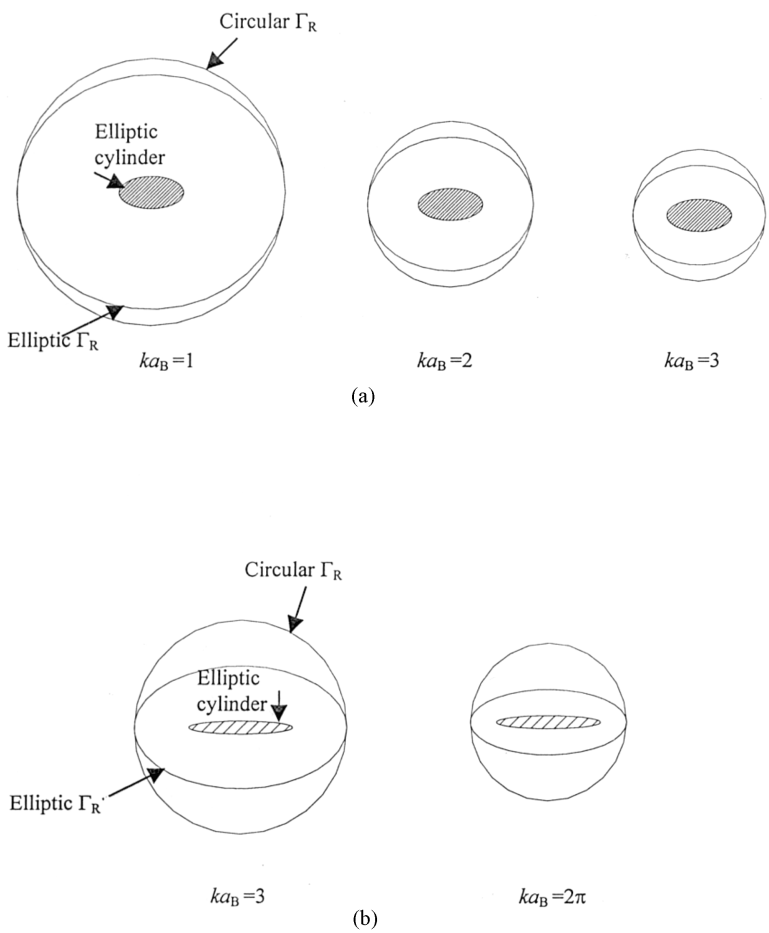

Figure 6. Modelling domain for BGT and elliptic boundary dampers for elliptic cylinders. (a) Elliptic cylinder of aspect ratio 2. (b) Elliptic cylinder of aspect ratio 8.

forces and moments are obtained as integrals, the wave run-up is a field quantity (see Equation (45)) and both together should provide a good basis to assess the performance of the elliptic dampers. The results of the three elliptic dampers are provided in terms of percentage differences in forces with respect to the results obtained using the BGT damper (i.e. on a circular Γ_R) as well as graphical plots of η. It may be noted that for $\theta = 0°$ and 180°, $F_y = M_x = 0$ and η is symmetric about the x-axis and for $\theta = 90°$ and 270°, $F_x = M_y = 0$ and η is symmetric about the y-axis. Also, since the percentage differences of F_x and M_y are always very close and the same is true of the (F_y, M_x) pair, the difference values of M_x and M_y have not been presented, except for one case for comparison with values from the literature.

The BGT-type dampers are based on the expansion of the far-field scattered/radiated waves in polar co-ordinates, whereas the elliptic dampers essentially imply that the waves are expanded in elliptic co-ordinates. Therefore, the question of what ellipse to choose for the boundary Γ_R becomes very important. In Grote and Keller [6], who solved acoustic scattering problems, confocal ellipses were chosen for numerical illustration. In general, the smaller the aspect ratio of the elliptic Γ_R, the better it is. This is because an ellipse with smaller aspect ratio is closer to a circle than a flatter ellipse, which has a larger aspect ratio. For a confocal ellipse, $a_R = a_B + c$, $b_R = \sqrt{a_R^2 - a_B^2 + b_B^2}$ and $d = b_R - b_B$. However, from a practical viewpoint, a 'parallel' ellipse (i.e. $c = d$), if it works, is the best choice for Γ_R. For a parallel ellipse, the aspect ratio is always larger than that of a confocal ellipse and hence it is inherently worse than a confocal ellipse as a choice of Γ_R. On the other hand, a parallel ellipse is attractive for two reasons. Firstly, it is flatter than a confocal ellipse and therefore the finite element domain could be much smaller. Secondly, in the case of an arbitrary elongated body, which is not an ellipse, the word 'confocal' means little and it has to be interpreted probably in terms of an 'equivalent ellipse' circumscribing the body. Instead, once c/L is chosen, c can be laid off from the longitudinal extremities of the body and an equal d ($= c$) can be laid off from the transverse extremities of the body and the 'parallel' ellipse constructed, though not in an exact sense of the term. In the numerical investigations, attention is paid to the 'reasonable' choice of the ellipse for Γ_R.

The results of the forces and moments for the elliptic cylinder of aspect ratio 2 are presented in Table I. For $\theta = 0°$, F_x and M_y were reported in Clark *et al.* [11] and therefore, these values are included in this table. For $\theta = 45°$ and 90°, only force values are presented. It may be observed that for all these angles and wave parameters, all elliptic dampers give virtually identical results as the BGT damper. This is because, even for a parallel ellipse chosen in all cases ($c = d$), the aspect ratios of Γ_R (a_R/b_R) are close to unity. Clearly, an elliptic cylinder of aspect ratio 2 is too small to bring out the effectiveness and relative performance of the elliptic boundary dampers and hence an elliptic cylinder of aspect ratio 8 representing an elongated geometry is studied in detail.

The results of forces for the elliptic cylinder of aspect ratio 8 by using the BGT damper are presented in Table II and the percentage differences w.r.t. these values by using the elliptic dampers are summarized in Table III. This table shows that for $\theta = 0°$, all elliptic dampers work equally well for $ka_B = 3$ whereas for $ka_B = 2\pi$, the D2 damper is clearly superior followed by the GK damper which is as expected. For $\theta = 45°$, all elliptic dampers work equally well in predicting F_x for $ka_B = 3$, whereas for $ka_B = 2\pi$, the D2 damper is clearly superior followed by the D1 damper. On the other hand, for $\theta = 45°$ and 90°, both the D1 and D2 dampers predict

Table I. Forces and moments for an elliptic cylinder of aspect ratio 2[a]

θ (°)	Force/ moment	Damper	$ka_B = 1$, $a_R/b_R = 1.14$		$ka_B = 2$, $a_R/b_R = 1.24$		$ka_B = 3$, $a_R/b_R = 1.32$	
			Amplitude	Phase	Amplitude	Phase	Amplitude	Phase
0	F_x	Clark *et al.* [11]	56.22	−80.77	32.89	86.85	13.35	42.73
		BGT	56.17	−80.73	32.90	86.81	13.34	42.71
		GK	56.15	−80.77	32.88	86.85	13.18	42.84
		D1	56.08	−80.67	32.93	86.85	13.23	42.73
		D2	56.14	−80.73	32.89	86.84	13.22	42.84
	M_y	Clark *et al.* [11]	52.01	−80.73	25.07	86.79	8.06	42.77
		BGT	51.92	−80.73	25.06	86.81	8.05	42.71
		GK	51.90	−80.76	25.04	86.86	7.95	42.84
		D1	51.84	−80.66	25.08	86.85	7.98	42.74
		D2	51.89	−80.73	25.06	86.85	7.97	42.83
45	F_x	BGT	41.69	−80.74	29.60	87.02	19.52	60.20
		GK	41.67	−80.78	29.60	87.08	19.41	60.67
		D1	41.62	−80.68	29.62	87.08	19.41	60.93
		D2	41.67	−80.74	29.60	87.03	19.45	60.23
	F_y	BGT	90.49	−60.93	45.87	−54.61	17.84	−76.70
		GK	90.17	−60.93	45.55	−55.04	17.83	−77.06
		D1	90.21	−60.86	45.78	−54.87	17.88	−76.79
		D2	90.38	−60.96	45.91	−54.73	17.86	−76.62
90	F_y	BGT	134.09	−60.96	79.97	−55.84	51.58	−76.03
		GK	133.61	−60.96	79.44	−56.27	51.50	−76.44
		D1	133.67	−60.89	79.81	−56.07	51.59	−76.13
		D2	133.92	−60.99	80.02	−55.96	51.63	−76.08

[a] $c/L = 0.5$ for circular Γ_R, $c/L = d/L = 0.5$ for elliptic Γ_R, force in kN, moment in kNm, phase in degrees, all dampers are of second-order.

F_y reasonably well, the D2 damper still being superior. The GK damper has large errors for these cases.

The wave run-up and its phase around the elliptic cylinder at the free surface are plotted in Figures 7–10 for $\theta = 45°$ with $ka_B = 3$ and for $\theta = 0°$, 45° and 90° with $ka_B = 2\pi$. For $ka_B = 3$ and $\theta = 45°$ (see Figure 7), it is seen that both the D1 and D2 dampers perform equally well and the GK damper is inferior except near the region $\psi = 0°$ and 180°. For $ka_B = 2\pi$, all dampers produce almost identical results of the wave run-up and phase for $\theta = 0°$. The reason is that the wave scattering effect is very small for this angle of wave incidence, as is evident from Figure 11, where the scattered wave elevations for three values of θ are presented. For $\theta = 45°$ and 90° (see Figures 9 and 10), the GK damper has large errors in both run-up and phase, whereas both the D2 and D1 dampers perform reasonably well, though the D2 damper is decidedly superior.

At this stage, it is adequately shown that the D2 damper performs best and there is no need to use the GK (which performs poorly for $\theta = 45°$ and 90°) and D1 (which performs poorly

Table II. Forces on an elliptic cylinder of aspect ratio 8 using second-order BGT damper[a]

θ (°)	Force	$ka_B = 3,\ d/L = 0.75$		$ka_B = 2\pi,\ d/L = 1.38$	
		Amplitude	Phase	Amplitude	Phase
0	F_x	0.7855	77.47	0.2202	67.57
45	F_x	1.3887	80.86	0.2733	−84.09
	F_y	5.2122	−12.86	1.2348	−17.42
90	F_y	12.9016	−24.10	6.3178	−39.93

[a] $c/L = 0.5$, force in kN, phase in degrees.

for $\theta = 0°$) dampers. Therefore, the damper D2 in conjunction with a parallel ellipse with $c/L = 0.5$ is a good choice in engineering applications.

For many practical ocean engineering problems, the maximum required ka_B value is around 3. For these problems, parallel ellipse as Γ_R will work well with the attendant computational advantage. Table IV shows a comparison of typical computer storage and CPU time requirements. Use of elliptic Γ_R leads to a saving of about 50 per cent in storage and about 60 per cent in computation time.

For problems with low values of ka_B (≤ 1), the use of elliptic dampers is not attractive because there is little difference in the size of the computational domain between the circular and elliptic (either parallel or confocal) boundaries.

Table III. Percentage differences in forces on an elliptic cylinder of aspect ratio 8 for second-order GK, D1 and D2 dampers[a]

θ (°)	Force	Damper	$ka_B=3,\ c/L=d/L=0.5$		$ka_B=2\pi,\ c/L=d/L=0.5$	
			Amplitude	Phase	Amplitude	Phase
0	F_x	GK	0.69	1.29	2.59	3.46
		D1	0.66	1.01	5.82	2.57
		D2	0.23	0.52	1.09	1.03
45	F_x	GK	0.55	0.67	0.07	−206.09
		D1	0.06	0.64	2.19	1.73
		D2	0.04	0.23	−0.23	−0.83
	F_y	GK	12.20	15.39	−8.27	−49.25
		D1	−2.94	9.25	−3.38	−25.48
		D2	1.63	7.45	5.16	17.17
90	F_y	GK	11.05	−12.42	−14.71	20.61
		D1	−0.98	3.78	−1.95	1.61
		D2	−0.11	3.07	−1.60	1.30

[a] Percentages are w.r.t. values in Table II, negative sign indicates values smaller than those in Table II.

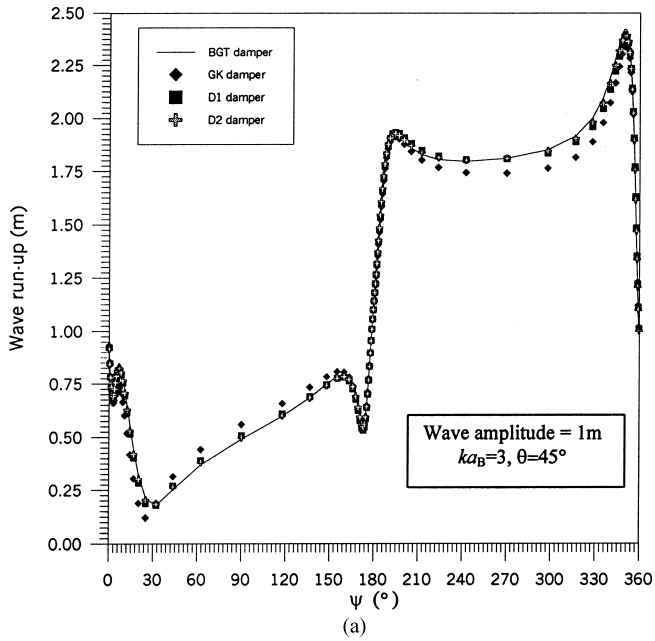

(a)

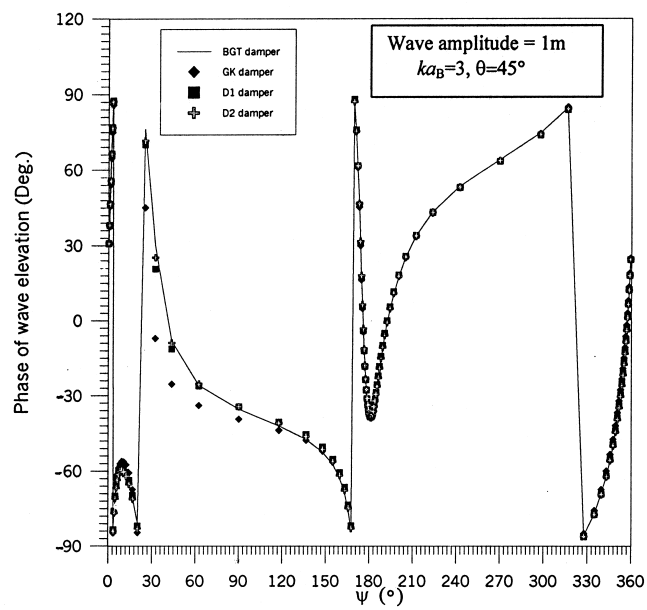

(b)

Figure 7. Wave run-up (a) and phase (b) for an elliptic cylinder of aspect ratio 8 using second-order BGT, GK, D1 and D2 dampers (for circular boundary $c = 0.5L$ and for elliptic boundary $c = d = 0.5L$).

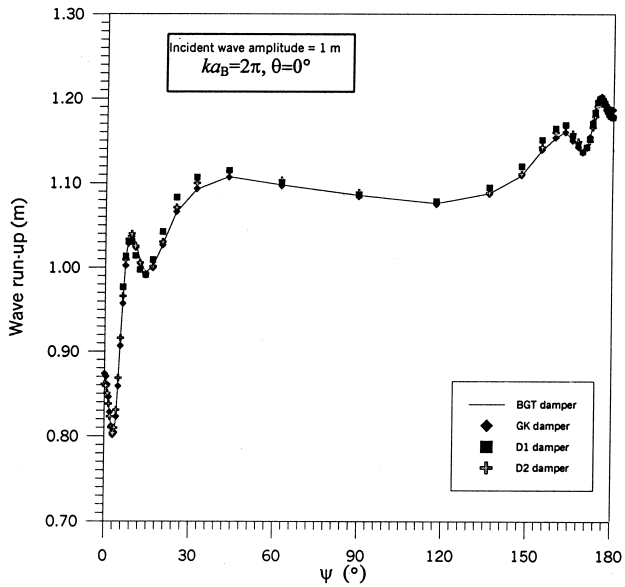

(a)

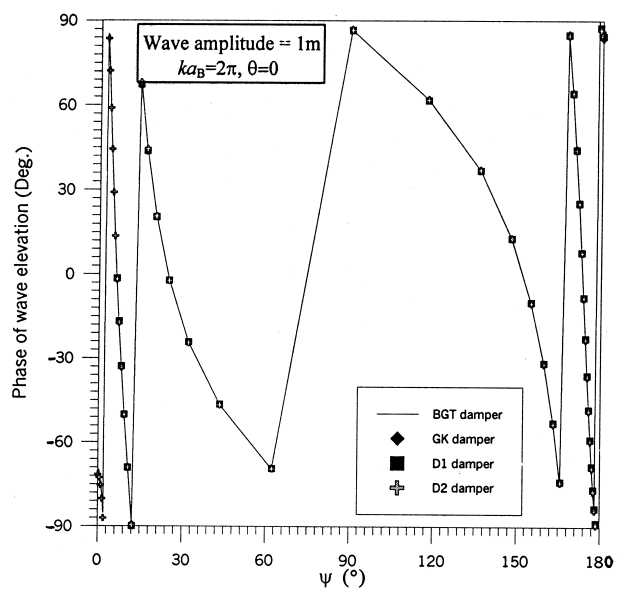

(b)

Figure 8. Wave run-up (a) and phase (a) for an elliptic cylinder of aspect ratio 8 using second-order BGT, GK, D1 and D2 dampers (for circular boundary $c = 0.5L$ and for elliptic boundary $c = d = 0.5L$).

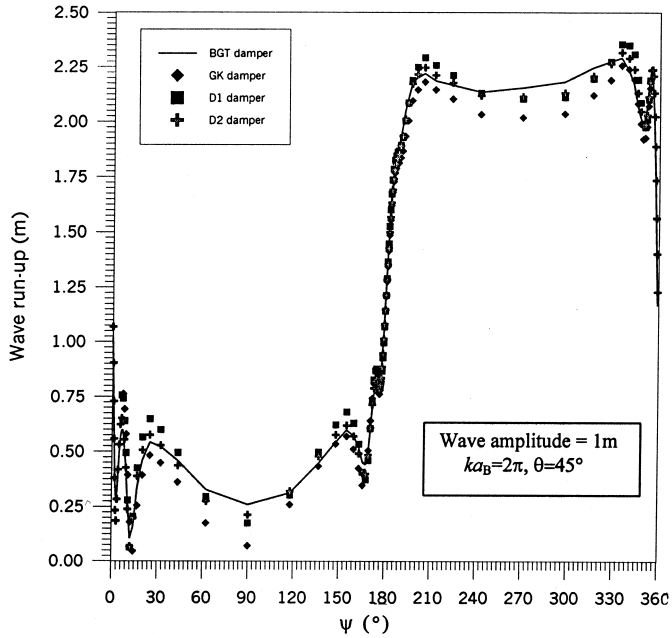

(a)

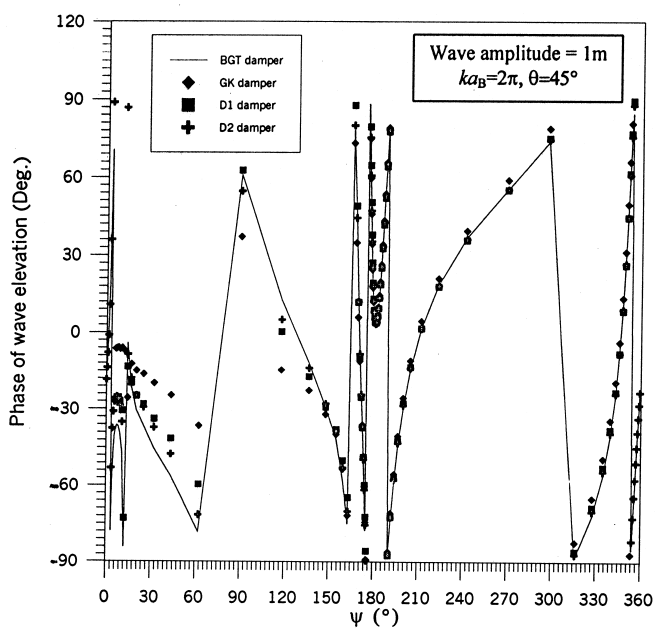

(b)

Figure 9. Wave run-up (a) and phase (b) for an elliptic cylinder of aspect ratio 8 using second-order BGT, GK, D1 and D2 dampers (for circular boundary $c = 0.5L$ and for elliptic boundary $c = d = 0.5L$).

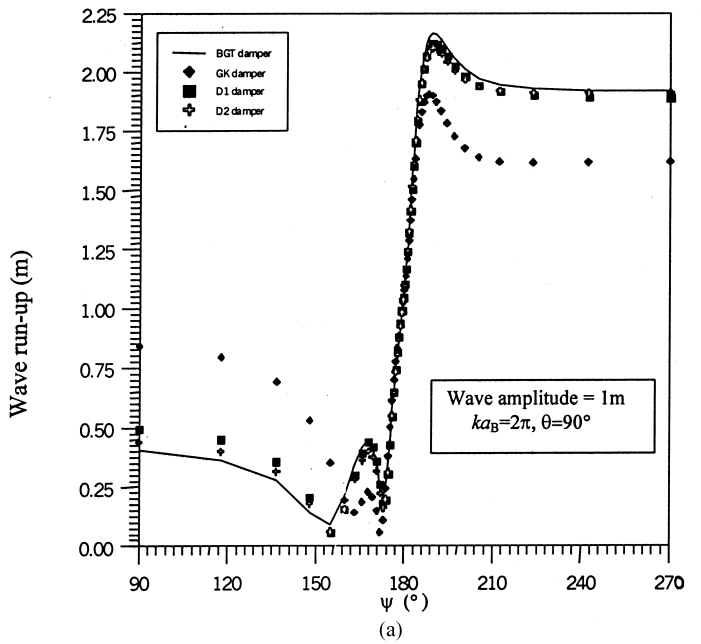

Figure 10. Wave run-up (a) and phase (b) for an elliptic cylinder of aspect ratio 8 using second-order BGT, GK, D1 and D2 dampers (for circular boundary $c = 0.5L$ and for elliptic boundary $c = d = 0.5L$).

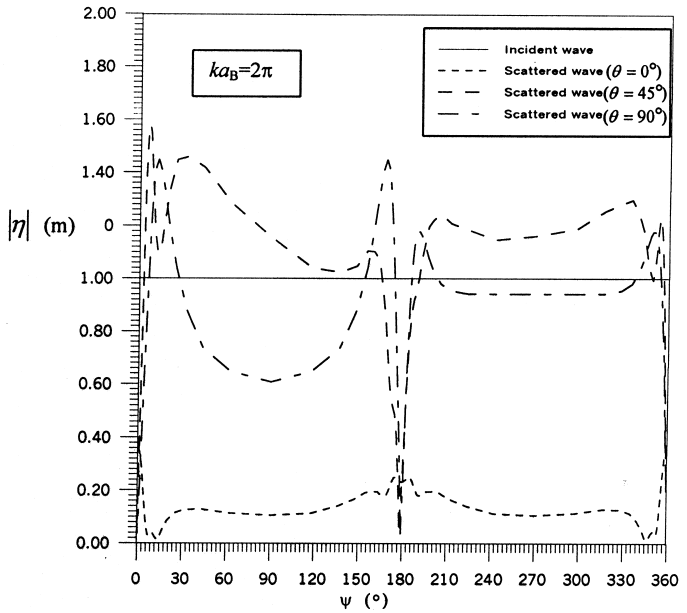

Figure 11. Comparisons of incident and scattered wave elevations.

It is well known that the first-order counterpart of the BGT damper is inferior in performance and so will be the case for the elliptic dampers treated in this paper. The difference in computational effort between first- and second-order dampers is insignificant and hence there is no real need to use the first-order dampers. However, all elliptic dampers of both hence there is no real need to use the first-order dampers. However, all elliptic dampers of both orders have been implemented in the finite element code developed in this study. To demonstrate this, a comparison between first- and second-order D2 dampers using the same finite element mesh is shown in Figure 12 for one of the cases.

Table IV. Comparison of computer storage and time requirements for BGT and elliptic dampers[a]

ka_B	No. of nodes × semi-bandwidth		Storage requirement (Mb)		Time requirement (s)		Percentage saving for elliptic damper	
	BGT damper	Elliptic damper	BGT damper	Elliptic damper	BGT damper	Elliptic damper	Storage	Time
3	6336 × 755	4128 × 496	86.88	43.91	456.16	189.05	49.46	58.55
2π	8554 × 805	5232 × 567	128.75	59.35	710.52	274.68	53.90	61.34

[a] Platform used for computation is Pentium PC 330 MHz.

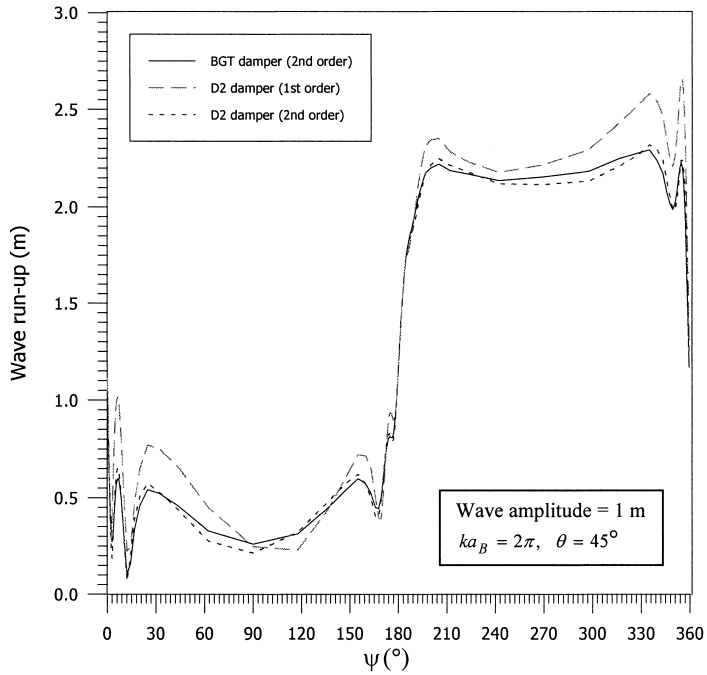

Figure 12. Comparison of wave run-up for an elliptic cylinder of aspect ratio 8 and $ka = 6.28$ using first- and second-order D2 dampers ($c/L = d/L = 0.5$) and second-order BGT damper.

8. CONCLUSION

The elliptic damper for general wave incidence (D2) introduced in this paper seems to have potential for application in diffraction-radiation problems of elongated floating bodies. It may also find application in two-dimensional acoustic and electromagnetic scattering problems using FEM and FDM. The question of appropriate size of the elliptic boundary is addressed in detail only for the problem of diffraction of water waves. It has to be worked out afresh for water wave problems when radiation combines with diffraction as also for the acoustic and electromagnetic scattering problems.

9. NOTE ADDED IN PROOF

Considering the coefficient of the D2 damper in Equation (34b), in order to represent the damper equation as a quadratic functional, first the variable r (see Equation (31)) has to be approximated by a representative constant value for an element, which might be accurate enough provided the finite elements are sufficiently small. Then with this assumption, Equation (37) is also valid for the D2 damper and thus, the functional $I_R(\phi)$ in Equation (36a) can be

adopted for FE modelling. The numerical results clearly show the acceptability of this approximation.

REFERENCES

1. Givoli D. Nonreflecting boundary conditions. *Journal of Computational Physics* 1991; **94**: 1–29.
2. Emson CRI. Methods for the solution of open-boundary electromagnetic field problems. *IEEE Proceedings A* 1988; **135**(3): 151–158.
3. Bayliss A, Gunzburger E, Turkel E. Boundary condition for the numerical solution of elliptic equations in exterior regions. *SIAM Journal of Applied Mathematics* 1982; **42**: 430–451.
4. Bando K, Bettes P, Emson C. The effectiveness of dampers for the analysis of exterior scalar wave diffraction by cylinders and ellipsoids. *International Journal for Numerical Methods in Fluids* 1984; **4**: 599–617.
5. Krishnankutty P, Vendhan CP. Three dimensional finite element analysis of the diffraction-radiation problems of hydrodynamically compact structures. *Marine Structures* 1995; **8**: 525–542.
6. Grote MJ, Keller JB. On nonreflecting boundary conditions. *Journal of Computational Physics* 1995; **122**: 231–243.
7. Burnett DS, Holford RL. Prolate and oblate spheroidal acoustic infinite element. *Computer Methods in Applied Mechanics and Engineering* 1998; **158**(1–2): 117–141.
8. Burnett DS, Holford RL. Ellipsoidal acoustic infinite element. *Computer Methods in Applied Mechanics and Engineering* 1998; **164**(1–2): 49–76.
9. Mei CC. *The Applied Dynamics of Ocean Surface Waves*. Wiley: New York, 1983.
10. McLachlan NW. *Theory and Application of Mathieu Functions*. Dover Publications: New York, 1964.
11. Clark PJ, Bettes P, Hearn GE, Downie MJ. The application of finite element analysis to the solution of Stokes diffraction problems. *International Journal for Numerical Methods in Fluids* 1991; **12**: 343–367.
12. Zienkiewicz OC, Taylor RL. *The Finite Element Method: Solid and Fluid Mechanics Dynamics and Non-Linearity*, vol. II. McGraw-Hill: London, 1991.
13. Zienkiewicz OC, Taylor RL. *The Finite Element Method: Basic Formulation and Linear Problems*, vol. I. McGraw-Hill: London, 1989.
14. Chakrabarti SK. *Hydrodynamics of Offshore Structures*. Computational Mechanics Publications: Southampton, 1987.

